Engineering Science and Technology, an International Journal xxx (xxxx) xxx

HOSTED BY

Contents lists available at ScienceDirect

Engineering Science and Technology, an International Journal

journal homepage: www.elsevier.com/locate/jestch

Full Length Article

Numerical and experimental investigation of cutting forces in turning of Nimonic 80A superalloy

Mehmet Erdi Korkmaz [a,*], Nafiz Yaşar [b], Mustafa Günay [a]

[a] Department of Mechanical Engineering, Faculty of Engineering, Karabük University, Karabük, Turkey
[b] Yenice Vocational High School, Karabük University, Karabük, Turkey

ARTICLE INFO

Article history:
Received 2 December 2019
Revised 15 January 2020
Accepted 4 February 2020
Available online xxxx

Keywords:
Nimonic 80A
Johnson-Cook Parameters
Turning
Simulation
Finite Element Metho

ABSTRACT

The study presents the machinability of Nimonic 80A superalloys depending on the cutting forces in both the turning experiments and simulations by finite element method (FEM) in order to approve the precision of the predetermined Johnson-Cook (JC) parameters from our previous study. In the first part of the paper, the turning experiments have been performed on Nimonic 80A superalloy with coated carbide tools to determine the cutting forces namely main cutting force, feed force and radial force. Three different cutting parameters namely depth of cut, cutting speed and feed rate have been used with three levels. The effect levels of the cutting parameters on cutting forces have been also determined with the analysis of variance (ANOVA) at 95% confidence level. Secondly, predetermined JC material model parameters have been inputted into the software running by FEM. Thereafter, the turning simulations have been performed by FEM with the same cutting conditions as experimental ones. According to ANOVA results, depth of cut is the most important parameter on Fc and Ff while feed rate is the most important factor on the Fr. Through the closer results (the mean of 6.45% deviation) of cutting forces between the experiments and simulations, the JC parameters of the material and the boundary conditions of the simulations have been approved with high accuracy.

1. Introduction

In machining processes, excesses on the workpiece may be discarded using a suitable machine tool and insert so that the workpiece can reach the desired size and surface quality. In this process; the relationship between the independent variables such as cutting parameters (cutting depth, feed rate, cutting velocity), cutting fluid, workpiece material, tool material, tool geometry, machine tool and the dependent variables such as cutting forces, surface quality, cutting tool life, cutting temperature should be evaluated well [1–5]. The selection of the machining parameters for both the machining method and materials type has been considered by many researchers for years and is still investigated to determine the optimum cutting conditions. Recently, it is obvious that cutting simulations based on finite element (FE) method is used to predict the machinability parameters such as cutting forces, temperature, cutting tool stresses for hard to machine materials [6,7].

Nickel-based superalloys are generally known as the materials that are resistant to environmental conditions and exhibit the required strength under operating conditions of 260 °C−1200 °C [8–11]. These materials, especially Nimonic80A are commonly used in turbine engines [12], automotive industries [13], power units, furnaces and also in the manufacturing of fasteners parts [14]. Nickel-based superalloy, instead, is amongst the difficult-to-cut machine owing to its high thermo-mechanic property [15–20]. Specifically, because of the fact that the investigation on the cutting process is complicated, FE modeling of any machining process is applicable as an alternate solution technique [21–30]. During the chip formation process; tremendous improvements have been provided by means of finite element models that help to predict the cutting force, surface quality, temperatures, and stresses value in machining processes [31–38]. Hence, the machining condition can be accustomed to the cutting process and it is likely to make a considerable influence to reduce the total expense by reducing tooling cost [39]. Within this context, the finite element models became vital tools in researches of engineering design and manufacturing processes.

Numerous constitutive material models are intentional presenting high strain behavior at a wide range of strain rates and temperatures to model the materials appropriately in simulation packages

* Corresponding author.
E-mail address: merdikorkmaz@karabuk.edu.tr (M.E. Korkmaz).
Peer review under responsibility of Karabuk University.

https://doi.org/10.1016/j.jestch.2020.02.001
2215-0986/

Please cite this article as: M. E. Korkmaz, N. Yaşar and M. Günay, Numerical and experimental investigation of cutting forces in turning of Nimonic 80A superalloy, Engineering Science and Technology, an International Journal, https://doi.org/10.1016/j.jestch.2020.02.001

[40,41]. The models are Zerili-Armstrong, JC model, Steinberg-Guanian model and it is highlighted that the JC model is commonly applied for several FE software [40]. Numerous researches were completed about the determination of JC parameters [42–47]. The authors highlighted that JC models are more applicable than other constitutive models. They also indicated that the tensile or compression test may be useful depends upon their usage areas. With this information, it is clearly seen that there is no FE simulation for any plastic deformational process such as milling, turning, deep drawing, crash test, etc. of Nimonic 80A superalloy. Unlike other studies, the novelty of this study is to investigate the machinability of the Nimonic 80A superalloy depending on the cutting forces in both turning experiments and the simulations by FEM in order to verify the accuracy of the predetermined JC parameters from our previous study.

2. Material and method

The Nimonic 80A superalloy has *C, Si, Mn, Al, Co, Fe, Ti, Cr* with the composition of 0.052, 0.06, 0.02, 1.35, 0.05, 0.8, 2.43, 19.2. The amount of Ni is about 70% for this material. Mechanical and physical properties of Nimonic 80A is shown in Table 1.

2.1. Turning experiments

In the turning process, the Nimonic 80A superalloy is used as a workpiece material, as a result of the literature survey, on which no finite element modeling of the machining process has been performed before. The workpiece dimensions are Ø40 × 250 mm and the hardness of the material used in the tests is 290 HV. In the turning experiments, CNGN 120408-MS coated carbide cutting tools, by Kyocera, are used as inserts having tool nose radius (rε) of 0.8 mm. These inserts with MS (γ; chip breaker angle 19°) chip breaker geometry (Fig. 1a) are rigidly connected to the tool holder in the form of PCLNR 2525M12 with an approaching angle (χr) of 95° on the CNC lathe.

The levels of cutting parameters are determined based on the cutting tool manufacturer's recommendation and literature reviews. Three different levels of cutting depth (a), cutting velocity (V) and feed rate (f) are selected and given in Table 2. The turning experiments have been performed on a TC 35 Johnford CNC lathe with a Fanuc control unit according to the parameters.

Measuring of cutting forces is provided by a 9257B type dynamometer. The cutting force data perceived by the dynamometer is transferred to the computer using Kistler Type 5019B130 Multichannel Charge Amplifier using Type 2855A3A/D Board CIO-DAS 1602/12 data acquisition card and Kistler Type 2825A1-2 Dynoware software. The cutting forces components (Fig. 1b) are obtained by dynamometer and equipment mentioned above. The stages of the turning process are schematically shown in Fig. 2. The cutting forces have been evaluated by taking the average of the data obtained by turning operations 2 times according to the full factorial experiment design.

Table 2
The parameters and levels.

Turning Parameters	Level 1	Level 2	Level 3
a (mm)	0.5	1	1.5
V (m/min)	45	60	75
f (mm/rev)	0.1	0.2	0.3

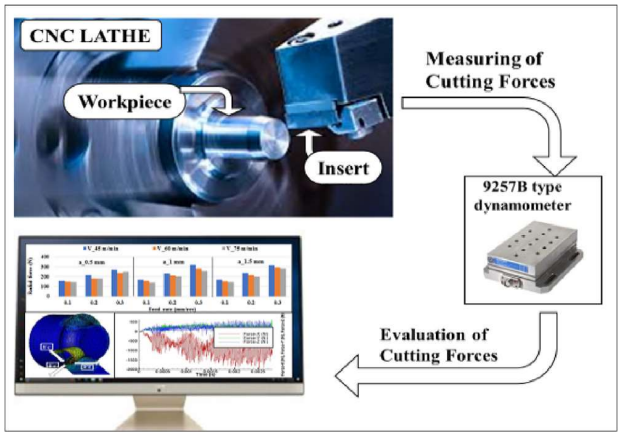

Fig. 2. The stages of the turning process.

Table 1
Mechanical and physical properties of Nimonic 80A [48].

Material	E (GPa)	T_m (°C)	α (10^{-6}/°C)	k (W/m°C)	υ	ρ (kg/m^3)	c_p (J/kg°C)
Nimonic 80A	183	1365	12.7	11.2	0.3	8190	448

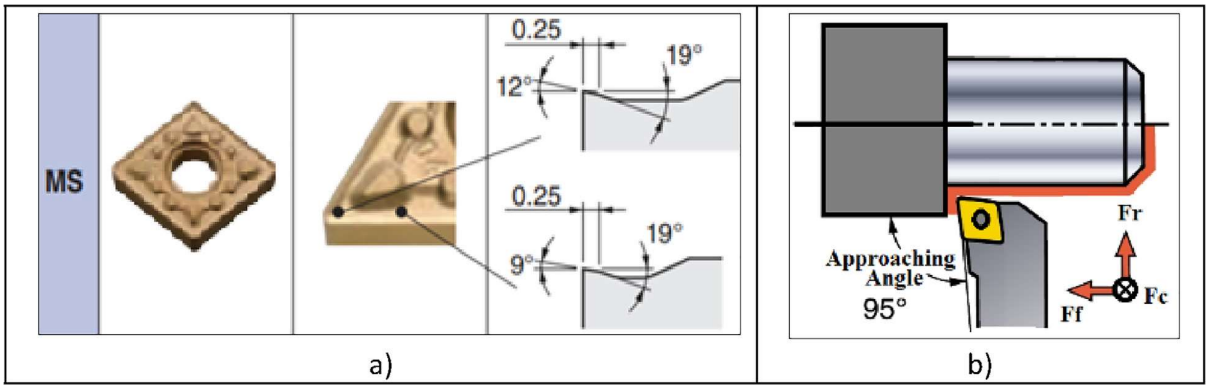

Fig. 1. a) Chip breaker geometry on the inserts, b) Cutting force components [49].

Please cite this article as: M. E. Korkmaz, N. Yaşar and M. Günay, Numerical and experimental investigation of cutting forces in turning of Nimonic 80A superalloy, Engineering Science and Technology, an International Journal, https://doi.org/10.1016/j.jestch.2020.02.001

2.2. Confirmation of JC parameters via FEM

ThirdWave Advantedge software has been used for turning simulations. The operations performed during the simulation are given below, respectively.

The dimensions of the workpiece used during the turning experiments are too much for the simulation and extend the analysis period. The smaller size of the workpiece in the simulation does not create any problem because the turning conditions will be the same in both the experiments and simulations. The cutting parameters required for the simulation are given in Fig. 3a. In addition, time-consuming will be less during the simulations. The dimensions of the workpiece processed in the simulations are given in Fig. 3b.

Another action required for simulations is cutting tool selection. After adopting the dimensions of the workpiece material and the turning conditions, the properties of the cutting insert are inputted. In the turning experiments, CNMG120408 coded coated carbide inserts are used. The codes C, N, M, G, 12, 04 and 08 indicate the insert shape, clearance angle, tolerance, insert type, size, thickness and nose radius, respectively (Fig. 4). M, G, 12 and 04 codes are not active in the analysis software, but the necessary features can be entered manually. In this section, the side rake angle, back rake angle and lead angle by the connection between the tool holder and the insert are also transferred to the software. In addition, the friction coefficient between the insert and the workpiece has been assumed to be 0.6 and the coating thickness has been adapted to the software as 3 μm. The insert parameters are shown in Fig. 4.

The process that needs to be done before the solution process is integrating the JC parameters of the Nimonic 80A superalloy that has been already predetermined [48] into the software. If any material is selected from the software database, the material could be selected when defining the workpiece. However, since the Nimonic 80A superalloy used does not have any constitutive parameters, they can be adopted later. By this means, any machining operation of this alloy can be performed with this software. When entering the material parameters section of the workpiece, the heat transfer properties and then the elastic properties are asked (Table 1). Finally, the program can be run after the Johnson-Cook parameters in Table 3 are entered (Fig. 5).

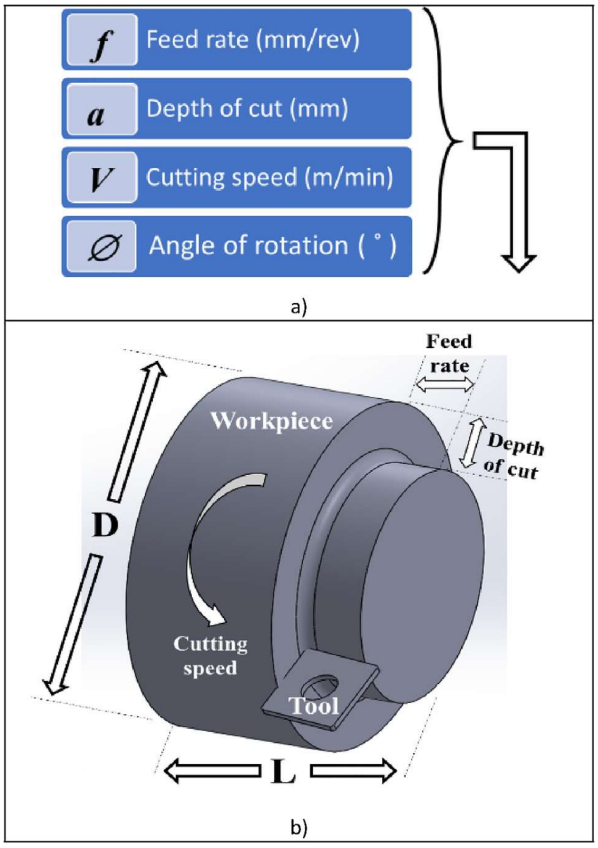

Fig. 3. Turning simulations, a) Turning conditions, b) Dimensions of the workpiece.

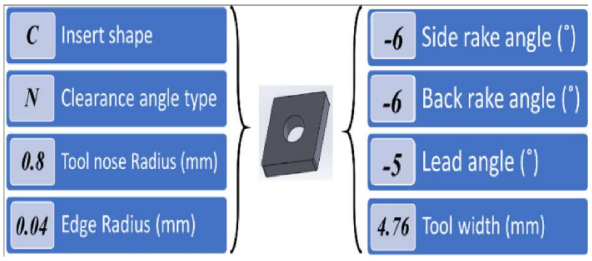

Fig. 4. The insert parameters.

After adapting the JC parameters to the software, the element type and element size (mesh structure) to be used in solid models have been determined for the type of the tool and tool holder. Three dimensional 10-node quadratic four-sided elements have been used for the cutting tools and workpieces used in the experiments. The mesh element sizes are applied to the tip of the inserts more intensively (minimum element size = 0.1 mm) and less frequently (maximum element size = 3 mm) in other parts. In order to determine the most suitable element size, mesh sensitivity analysis has been performed to obtain the optimum mesh size which will give a good balance between experimental and simulational main cutting force values. Simulational Fc values have been obtained over a period of time when the cutting simulation is stable. Table 4 shows the average of main cutting force values corresponding to the element size used for a sample experiment (V = 60 m/min, f = 0.3 mm/rev and a = 1 mm). As it is understood from this table, when the element size is reduced from 0.1 mm to 0.05 mm, there is a slight difference in the force value. In this case, it has been decided that the element size would be 0.1 mm so that the analysis time did not extend further. The mesh structure of the workpiece and the cutting insert are demonstrated in Figs. 6 and 7, respectively.

3. Results and discussion

3.1. Turning experiments

3.1.1. Main cutting force (Fc)

F_c values which are important at the primary level in terms of energy consumption in turning are firstly taken into account in the analysis of the cutting forces. The F_c values have about a 50% increase with a 100% increase of the feed rate while this increased rate is about 30% by the 50% increase of the feed rate as shown in Fig. 8. This variation in the main cutting force is similar for each cutting depth. The F_c values have about %65 increase with increasing cutting depth as 100%, while %35 increase by increasing cutting

Table 3
JC parameters of Nimonic 80A [48].

Material	A (MPa)	B (MPa)	n	C	m	$\dot{\varepsilon}_0(s^{-1})$
Nimonic 80A	501	860	0.82	0.0122	1.42	10^{-3}

Please cite this article as: M. E. Korkmaz, N. Yaşar and M. Günay, Numerical and experimental investigation of cutting forces in turning of Nimonic 80A superalloy, Engineering Science and Technology, an International Journal, https://doi.org/10.1016/j.jestch.2020.02.001

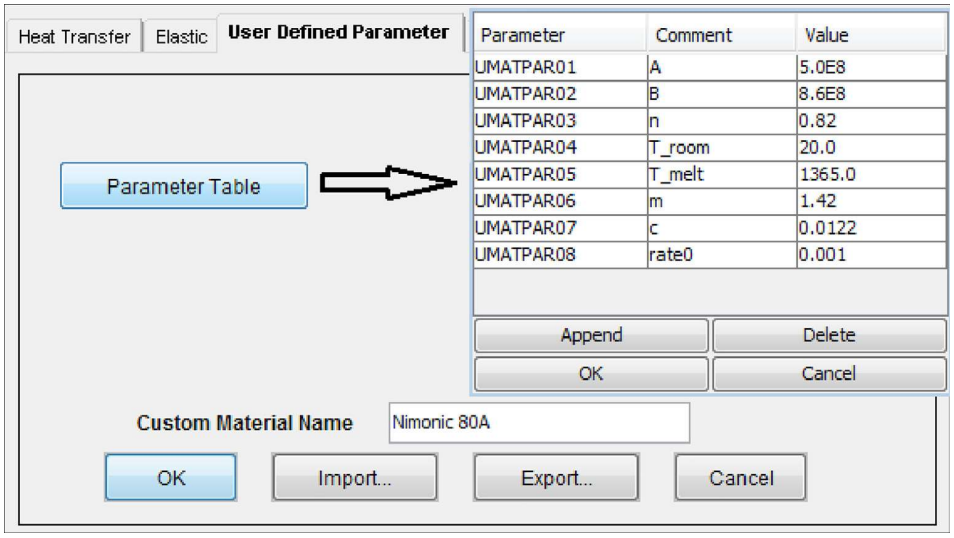

Fig. 5. The JC parameters of Nimonic 80A superalloy.

Table 4
Mesh-sensitivity for the Fc values.

Element size (mm)	Main cutting force (N)
1	805
0.7	818
0.3	828
0.1	834
0.05	835

depth as 50% (Fig. 8). This increasing trend in the F_c is also obtained for each feed rate. With the increasing depth of cut and feed rate, the tool-chip contact area and the volume of material removed increase, and hence the main cutting force increases [50,51]. On the other hand, there is a decreasing trend by increasing cutting velocity as expected but the decreasing ratio is slight as also seen from the result of variance analysis (Table 5). In general, the strength of the workpiece materials decreases by softening due to increasing temperature caused by high cutting velocity, leading to decrease in cutting forces. However, high strain hardening is generated in nickel-based superalloys at elevated temperatures [48,52,53]. Thus, high cutting velocity cannot reduce the cutting forces adequately in nickel-based superalloys. The minimum F_c value is measured as 242 N in cutting depth of 0.5 mm, feed rate of 0.1 mm/rev and cutting velocity of 45 m/min.

The experimental results are also evaluated with ANOVA with a 95% confidence level to determine the influences of parameters on machining outputs, namely F_c, F_r, F_f. According to ANOVA results, P values must be less than 0.05 to understand that the parameter is effective on the machining outputs. Table 5 indicates that the depth of cut is the most important parameter on F_c with 48.4% PCR (Percentage contribution ratio). It can be said that the feed rate and the interaction of f^*a are the secondary and the tertiary important parameters on the cutting force with 45.88% and 5.24% PCR, respectively. However, the other parameters have inconsiderable effects on the F_c.

3.1.2. Radial force (Fr)

The radial force (F_r) values which are generally the lowest one of the cutting force components in conventional cylindrical turning operation. The F_r values are lower than the F_f values for the cutting depth of 1 and 1.5 mm as expected, but higher for the cutting depth of 0.5 mm. Since the tool nose radius (0.8 mm) is higher than cutting depth, the radial force is higher due to chip formation occurs depending on ploughing effect as mentioned in Ref. [54]. It is valid only for the cutting depth of 0.5 mm that the F_r values have about 25% increase with increasing feed rate both from 0.1 to 0.2 mm/rev and from 0.2 to 0.3 mm/rev. This increased ratio is

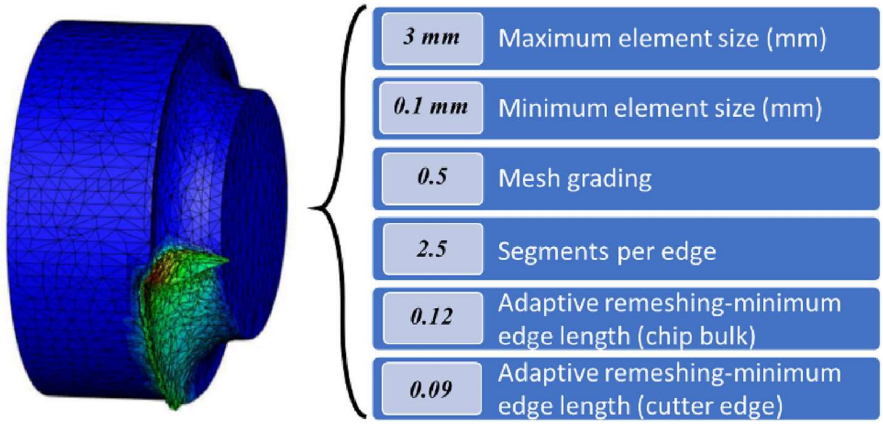

Fig. 6. The mesh structure for the workpiece.

Please cite this article as: M. E. Korkmaz, N. Yaşar and M. Günay, Numerical and experimental investigation of cutting forces in turning of Nimonic 80A superalloy, Engineering Science and Technology, an International Journal, https://doi.org/10.1016/j.jestch.2020.02.001

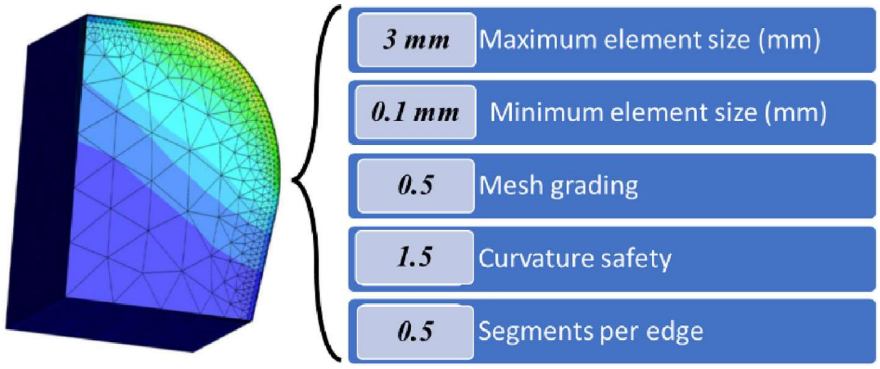

Fig. 7. The mesh structure for the insert.

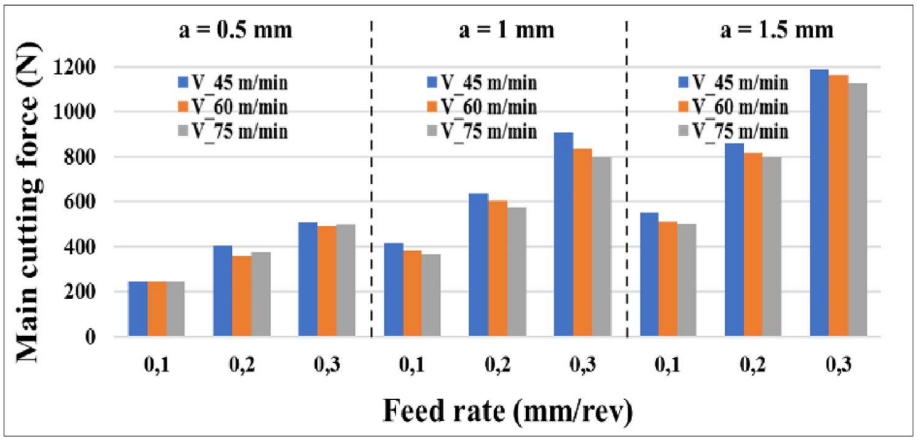

Fig. 8. The distribution of F_c values.

Table 5
ANOVA results for F_c.

Parameter	Degree of Freedom	Sum of Square	Mean Square	F	P	PCR
V	2	13,672	6836	41.76	0.000	0.68
f	2	924,983	462,492	2825.38	0.000	45.53
a	2	983,396	491,698	3003.81	0.000	48.4
V*f	4	464	116	0.71	0.609	0.02
V*a	4	1510	378	2.31	0.146	0.07
f*a	4	106,490	26,622	162.64	0.000	5.24
Error	8	1310	164			0.06
Total	26	2,031,824				100

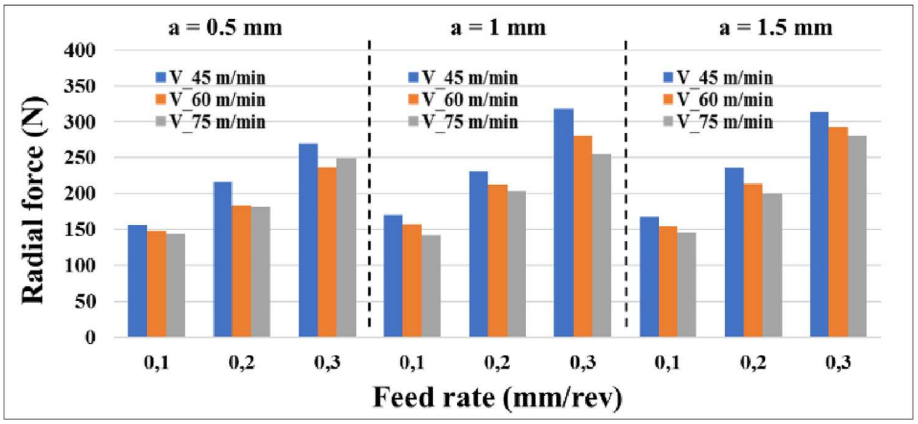

Fig. 9. The distribution of F_r values.

Please cite this article as: M. E. Korkmaz, N. Yaşar and M. Günay, Numerical and experimental investigation of cutting forces in turning of Nimonic 80A superalloy, Engineering Science and Technology, an International Journal, https://doi.org/10.1016/j.jestch.2020.02.001

50% by increasing the feed rate in the range 0.1–0.3 mm/rev for the cutting depth of 1 and 1.5 mm as shown in Fig. 9.

The F_r values have a little change by increasing the cutting depth (Fig. 9) as indicated in Ref [55]. As can be seen from Fig. 10, the tool-chip contact area and so the force distribution is smaller than that of other forces depending on approaching angle of the cutting tool. Therefore, the F_r component has a little increment by increasing cutting depth due to less change of the

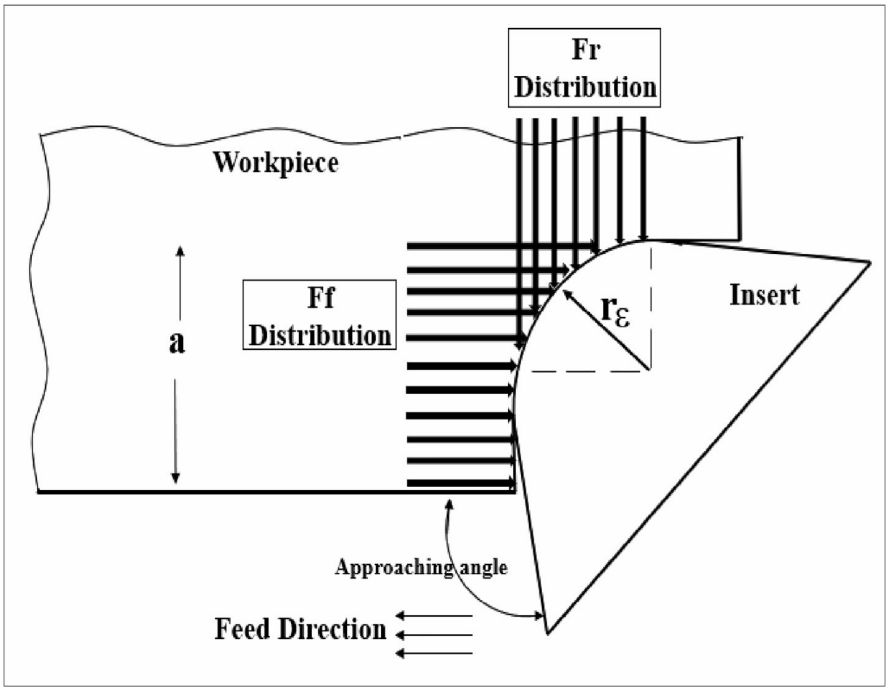

Fig. 10. Load distributions of Fr and Ff.

Table 6
ANOVA results for F_r.

Parameter	Degree of Freedom	Sum of Square	Mean Square	F	P	PCR
V	2	5596.1	2798.0	58.51	0.000	7.40
f	2	62,900	31450.0	657.63	0.000	83.15
a	2	5367.8	2683.9	56.12	0.000	7.10
*V***f*	4	318.3	79.6	1.66	0.250	0.42
*V***a*	4	75.2	18.8	0.39	0.808	0.10
*f***a*	4	999.8	250.0	5.23	0.023	1.32
Error	8	382.6	47.8			0.51
Total	26	75639.8				100

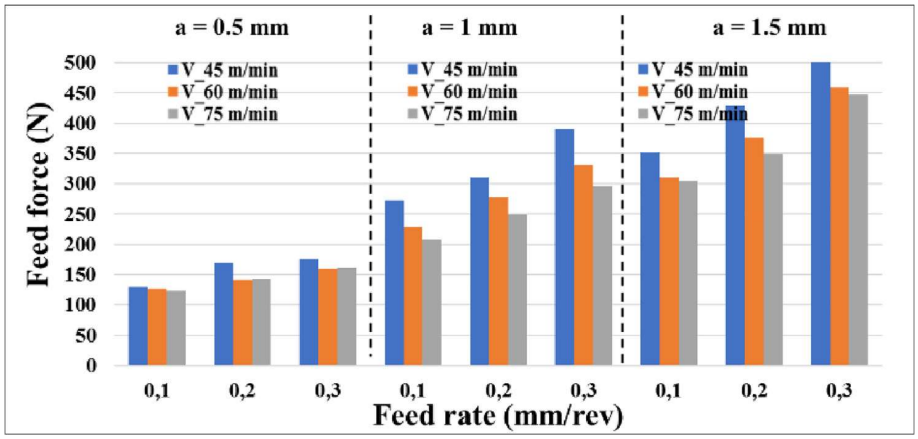

Fig. 11. The distribution of *Ff* values.

Please cite this article as: M. E. Korkmaz, N. Yaşar and M. Günay, Numerical and experimental investigation of cutting forces in turning of Nimonic 80A superalloy, Engineering Science and Technology, an International Journal, https://doi.org/10.1016/j.jestch.2020.02.001

Table 7
ANOVA results for *Ff*.

Parameter	Degree of Freedom	Sum of Square	Mean Square	F	P	PCR
V	2	12,426	6213	80.77	0.000	3.63
f	2	43,194	21,597	280.76	0.000	12.63
a	2	274,232	137,116	1782.51	0.000	80.14
*V*f*	4	407	102	1.32	0.341	0.12
*V*a*	4	1835	459	5.96	0.016	0.54
*f*a*	4	9452	2363	30.72	0.000	2.76
Error	8	615	77			0.18
Total	26	342,162				100

tool-chip contact area on F_r direction. Moreover, the F_r values are generally decreased by increasing cutting velocity as seen in Fig. 9. Even this decreasing tendency has become more obvious with increasing cutting depth and feed rate. This can be attributed to the reduction of friction forces in the second deformation zone due to the reduction of chip curve radius with increasing mentioned parameter above [56]. The minimum F_r value is obtained as 142.3 N in cutting depth of 0.5 mm, feed rate of 0.1 mm/rev and cutting velocity of 75 m/min.

According to ANOVA results, Table 6 shows that all cutting parameters are important for F_r, however, the feed rate is the most important factor on F_r with 83.15% PCR. Moreover, the cutting velocity is the secondary important parameter with 7.40% PCR while the cutting depth is the tertiary important parameter with 7.10% PCR. The other interaction parameters have inconsiderable effects on the F_r.

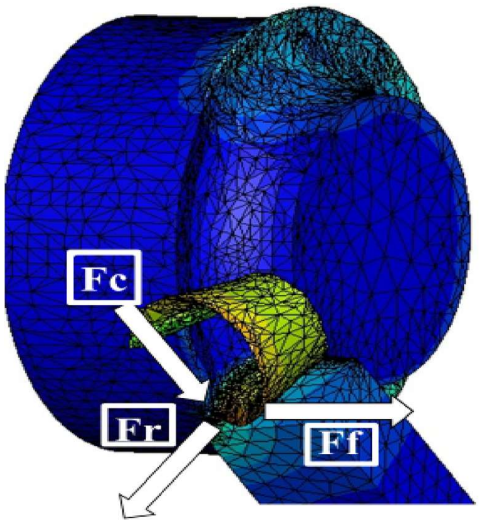

Fig. 12. The finite element analysis image of the cutting forces.

3.1.3. Feed force (Ff)

Feed force which is parallel to the feed direction can generally be up to about 50% of the force F_c [57]. In our study, the F_f/F_c value has been obtained as average of 47% by considering all the experiments. The relationship between the F_f and the F_r is explained in detail the part of the radial force (see section 3.1.2). It is valid for all the cutting depth that the F_f values have about an 18% increase with increasing feed rate both from 0.1 to 0.2 mm/rev and 24% increase by the feed rate from 0.2 to 0.3 mm/rev as seen from Fig. 11. The F_f values have a 90% increase by increasing the cutting depth from 0.5 to 1 mm while 35% increase from 1 to 1.5 mm. On the contrary, the cutting velocity has a reducing effect on the F_f values by 13% and %10 when it increases from 45 to 60 m/min and from 60 to 75 m/min, respectively (Fig. 11). The minimum F_f value is obtained as 123.7 N in cutting depth of 0.5 mm, feed rate of 0.1 mm/rev and cutting velocity of 75 m/min.

The most significant parameter on F_f is the cutting depth with 80.14% PCR (Table 7). The table also shown that the feed rate is the secondary important parameter with 12.63% PCR while the cutting velocity and the interaction of f^*a have 3.63% and 2.76% PCR. The interactions of V^*f and V^*a have an insignificant effect on F_f that is similar in F_r.

For the machining of Nimonic 80A alloy, the cutting force values are generally higher than the most of other nickel-based superalloys. The tendency can be referred that Nimonic 80A alloys retain their strength better than other superalloys in high temperatures which occur in machining operations [58]. As a whole, the increase in cutting forces with increasing feed rate (f) and cutting depth (a) is an expected situation in machining processes [59]. As a reason for this result, it is possible to show the increase in the tool-chip contact area and subsequently, the energy consumption increases in chip formation by the increase in f and a value. The cutting

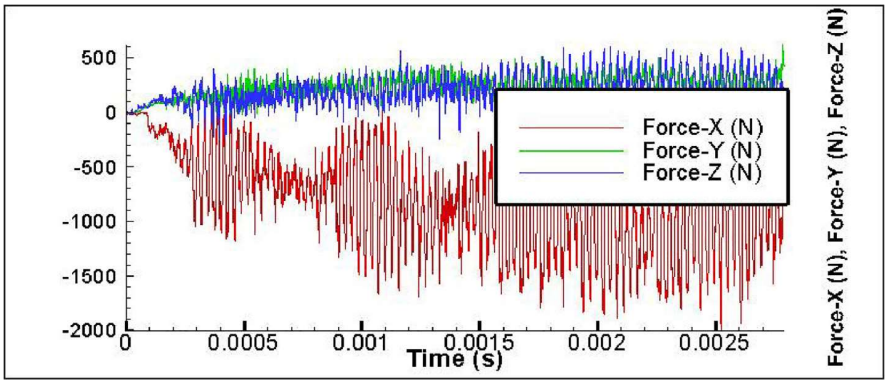

Fig. 13. The cutting force values for a sample test.

Please cite this article as: M. E. Korkmaz, N. Yaşar and M. Günay, Numerical and experimental investigation of cutting forces in turning of Nimonic 80A superalloy, Engineering Science and Technology, an International Journal, https://doi.org/10.1016/j.jestch.2020.02.001

forces display regular and expected tendencies, especially for the cutting depth of 1 and 1.5 mm. However, the irregular tendencies, in cutting depth of 0.5 mm (smaller than tool nose radius of 0.8 mm) can be referred to ploughing effect. The ploughing process is shown by the effect of minimum cutting depth, especially in F_r and F_f cutting force components. The increase in ploughing force results from uncut chip thickness or cutting depth which is less than a critical value ($a \geq r_\varepsilon$) [57], which is a micromachining process. Thus, unexpected tendencies for F_r and F_f are observed only in the minimum cutting depth.

Additionally, the multiple regression models are also developed to predict the cutting forces without needs for the experiments in these cutting conditions. The second-degree regression models for the cutting forces (F_c, F_r and F_f) are shown in Eqs. (1)–(3).

$$F_c = (7.33 - 0.0301 * V + 45.64 * f + 9.377 * a)^2 \quad (1)$$

$$F_r = (11.334 - 0.03164 * V + 21.036 * f + 0.874 * a)^2 \quad (2)$$

$$F_f = (8.696 - 0.0475 * V + 13.97 * f + 7.582 * a)^2 \quad (3)$$

The coefficients of determination (R^2) demonstrating the relation between independent (V, f, a) and dependent variables (F_c, F_r, F_f) are found as 0.9778, 0.9702 and 0.9638 for main cutting force, radial force and feed force, respectively.

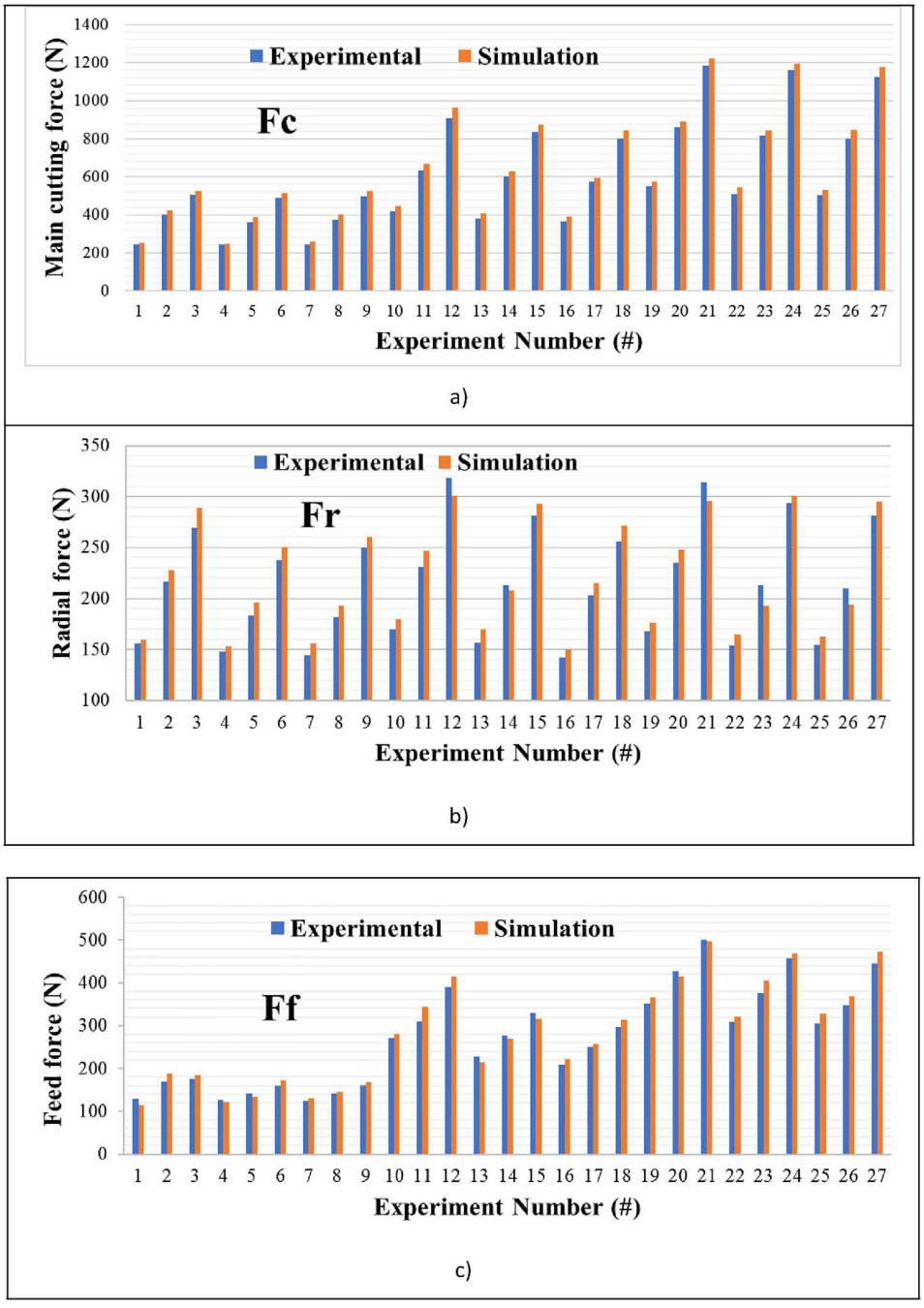

Fig. 14. The comparison of experimental and modeling results for; a) F_c, b) F_r, c) F_f.

Please cite this article as: M. E. Korkmaz, N. Yaşar and M. Günay, Numerical and experimental investigation of cutting forces in turning of Nimonic 80A superalloy, Engineering Science and Technology, an International Journal, https://doi.org/10.1016/j.jestch.2020.02.001

3.2. Comparison of turning experiments and simulations

At the end of finite element simulations, the sample image of the workpiece, insert and the chip is given in Fig. 12 beside cutting force components. Moreover, the force outputs obtained from the finite element analysis of a sample test is given in Fig. 13. The mean values of the forces are obtained by applying polynomial fit to the stabilized region of the force outputs.

The comparison of the results for the main cutting force (*Fc*), radial force (*Fr*) and feed force (*Ff*) obtained from the experimental and finite element analysis in the turning of the Nimonic 80A superalloy with coated carbide cutting tools is presented in Fig. 14.

When all the values in Fig. 14 are evaluated, the deviations between experimental and modeling results for the main cutting force, radial force and feed force are average 6.58%, 6.71% and 6.06%, respectively. The deviations between the experimental and modeling results have been mainly attributed to possible deviations in the JC model due to important variables such as microstructure or hardness modifications. At the same time, this result may be caused by the ploughing effect, when the cutting depth is smaller than the tool radius, that could not be precisely modeled in the FE software. However, the results generally show that the finite element model of the turning process based on predetermined Johnson-Cook parameters for F_c, F_r and F_f are developed with high accuracy. This situation proves that the model and some boundary conditions (the coefficient of friction, the coating thickness of inserts, etc.) assumed in the model are applicable and can be used in future researches.

4. Conclusion

The simulations based on FEA for any deformation processes are performed by using the default material model because there is no constitutive model of any new materials. The paper aimed to investigate the machinability of the Nimonic 80A superalloy depending on the cutting forces in both turning experiments and the simulations by finite element method in order to approve the accuracy of the predetermined JC parameters. The results obtained in the study are summarized below.

- Experimental F_c and F_f values obviously increased with the increasing feed rate and depth of cut. On the other hand, these cutting force components showed a decreasing tendency with increasing cutting speed as expected, but the effect of cutting speed is minimal level, as can be seen from the ANOVA results.
- F_r values increased with increasing feed rate as the other cutting force components. However, the F_r values showed a little change with the increasing depth of cut. This result is referred to a very small variation in force distributions due to the tool approaching angle.
- According to ANOVA results, the depth of cut is the most important parameter on F_c with 48.4% PCR, while the feed rate is the most important factor on the F_r with 83.15% PCR. Moreover, the most significant parameter on F_f is depth of cut with 80.14% PCR.
- The coefficients of determination (R^2) show the relation between independent (*V, f, a*) and dependent variables (F_c, F_r, F_f) and are found as 0.9778, 0.9702 and 0.9638 for main cutting force, radial force and feed force, respectively according to the multiple regression model.
- Between the experimental and simulation results, there are small deviations of 6.58%, 6.71% and 6.06% for the main cutting force, radial force and feed force, respectively. It has been concluded that these deviations are mostly due to the ignorance of microstructural alterations of the JC model and partly to the exact modeling of the ploughing effect in the simulation program.
- In conclusion, it can be probable to simulate FE model of any plastic deformation process, especially milling, drilling, ballistic or crash tests, etc. via JC parameters predetermined for Nimonic 80A nickel-based superalloy and confirmed by this study.

Declaration of Competing Interest

The authors declare that they have no known competing financial interests or personal relationships that could have appeared to influence the work reported in this paper.

Acknowledgement

The authors would like to thank Karabük University Coordinatorship of Scientific Research Projects for the financial support with project number KBUBAP-18-DR-005.

References

[1] M. Boy, N. Yaşar, I. Ciftci, Experimental investigation and modelling of surface roughness and resultant cutting force in hard turning of AISI H13 Steel, IOP Conf. Ser.: Mater. Sci. Eng. 161 (2016), https://doi.org/10.1088/1757-899X/161/1/012039.

[2] T. Kivak, G. Uzun, E. Ekici, An experimental and statistical evaluation of the cutting parameters on the machinability of hadfield steel, Gazi Univ. J. Sci. 29 (2016) 9–17.

[3] A. Zerti, M.A. Yallese, I. Meddour, S. Belhadi, A. Haddad, T. Mabrouki, Modeling and multi-objective optimization for minimizing surface roughness, cutting force, and power, and maximizing productivity for tempered stainless steel AISI 420 in turning operations, Int. J. Adv. Manuf. Technol. 102 (2019) 135–157, https://doi.org/10.1007/s00170-018-2984-8.

[4] M.D. Sharma, R. Sehgal, Modelling of machining process while turning tool steel with CBN tool, Arabian J. Sci. Eng. 41 (2016) 1657–1678, https://doi.org/10.1007/s13369-015-1864-x.

[5] M. Hanief, M.F. Wani, M.S. Charoo, Modeling and prediction of cutting forces during the turning of red brass (C23000) using ANN and regression analysis, Eng. Sci. Technol. Int. J. 20 (2017) 1220–1226, https://doi.org/10.1016/J.JESTCH.2016.10.019.

[6] L. Ma, C. Li, J. Chen, W. Li, Y. Tan, C. Wang, Y. Zhou, Prediction model and simulation of cutting force in turning hard-brittle materials, Int. J. Adv. Manuf. Technol. 91 (2017) 165–174, https://doi.org/10.1007/s00170-016-9642-9.

[7] T. Dorlin, G. Fromentin, J.P. Costes, Generalised cutting force model including contact radius effect for turning operations on Ti6Al4V titanium alloy, Int. J. Adv. Manuf. Technol. 86 (2016) 3297–3313, https://doi.org/10.1007/s00170-016-8422-x.

[8] H. Zhang, J.K. Li, Z.W. Guan, Y.J. Liu, D.K. Qi, Q.Y. Wang, Electron beam welding of Nimonic 80A: Integrity and microstructure evaluation, Vacuum 151 (2018) 266–274, https://doi.org/10.1016/J.VACUUM.2018.01.021.

[9] M.E. Korkmaz, P. Verleysen, M. Günay, Identification of Constitutive Model Parameters for Nimonic 80A Superalloy, Trans. Indian Inst. Met. 71 (2018) 2945–2952, https://doi.org/10.1007/s12666-018-1394-9.

[10] A.K. Parida, K. Maity, Experimental investigation on tool life and chip morphology in hot machining of Monel-400, Eng. Sci. Technol. Int. J. 21 (2018) 371–379, https://doi.org/10.1016/J.JESTCH.2018.04.003.

[11] A.K. Parida, K. Maity, Comparison the machinability of Inconel 718, Inconel 625 and Monel 400 in hot turning operation, Eng. Sci. Technol. Int. J. 21 (2018) 364–370, https://doi.org/10.1016/j.jestch.2018.03.018.

[12] M. Karadge, M. Preuss, P.J. Withers, S. Bray, Importance of crystal orientation in linear friction joining of single crystal to polycrystalline nickel-based superalloys, Mater. Sci. Eng., A 491 (2008) 446–453, https://doi.org/10.1016/J.MSEA.2008.04.064.

[13] D. Sahu, S.K. Sahu, T. Jadam, S. Datta, Electro-discharge machining performance of Nimonic 80A: an experimental observation, Arabian J. Sci. Eng. (2019), https://doi.org/10.1007/s13369-019-04112-1.

[14] N. Makuch, M. Kulka, Fracture toughness of hard ceramic phases produced on Nimonic 80A-alloy by gas boriding, Ceram. Int. 42 (2016) 3275–3289, https://doi.org/10.1016/J.CERAMINT.2015.10.119.

[15] A. Goswami, J. Kumar, Study of machining characteristics of Nimonic 80A using wire-cut, Int. J. Adv. Eng. Appl. 7 (2014) 73–81.

[16] A. Goswami, J. Kumar, Trim cut machining and surface integrity analysis of Nimonic 80A alloy using wire cut EDM, Eng. Sci. Technol. Int. J. 20 (2017) 175–186, https://doi.org/10.1016/J.JESTCH.2016.09.016.

[17] D. Sahu, S.K. Sahu, T. Jadam, S. Datta, Electro-discharge machining performance of Nimonic 80A: an experimental observation, Arabian J. Sci. Eng. 44 (2019) 10155–10167, https://doi.org/10.1007/s13369-019-04112-1.

[18] R.B. Penteado, T. de Rubia Fernanda, M.V. Oliveira, M.B. Silva Ribeiro, Application of taguchi method in turning process of a superalloy NIMONIC

Please cite this article as: M. E. Korkmaz, N. Yaşar and M. Günay, Numerical and experimental investigation of cutting forces in turning of Nimonic 80A superalloy, Engineering Science and Technology, an International Journal, https://doi.org/10.1016/j.jestch.2020.02.001

80A to improve the surface roughness, Int. J. Innovative Res. Eng. Manage. 2 (2015) 81–88.
[19] Patil J., Chavan V., Kadam S., Sadaiah M., Some Experimental Investigations on Turning of Nimonic 80A using Sialon Ceramic Inserts, 137 (2017) 259–264. doi:10.2991/iccasp-16.2017.41.
[20] R.B.R. Chekuri, R. Kalluri, J.K. Palakollu, R. Siriyala, Modeling and optimization of machining high performance nickel based super alloy Nimonic C-263 using die sinking EDM, Int. J. Mech. Eng. Rob. Res. 8 (2019) 196–201, https://doi.org/10.18178/ijmerr.8.2.196-201.
[21] W. Jomaa, O. Mechri, J. Lévesque, V. Songmene, P. Bocher, A. Gakwaya, Finite element simulation and analysis of serrated chip formation during high-speed machining of AA7075-T651 alloy, J. Manuf. Processes 26 (2017) 446–458, https://doi.org/10.1016/J.JMAPRO.2017.02.015.
[22] A. Malakizadi, S. Cedergren, I. Sadik, L. Nyborg, Inverse identification of flow stress in metal cutting process using response surface methodology, Simul. Model. Pract. Theory 60 (2016) 40–53, https://doi.org/10.1016/j.simpat.2015.09.009.
[23] M. Lotfi, S. Amini, M. Aghaei, Tool wear modeling in rotary turning modified by ultrasonic vibration, Simul. Model. Pract. Theory 87 (2018) 226–238, https://doi.org/10.1016/j.simpat.2018.07.007.
[24] B. Wang, Z. Liu, Shear localization sensitivity analysis for Johnson-Cook constitutive parameters on serrated chips in high speed machining of Ti6Al4V, Simul. Model. Pract. Theory 55 (2015) 63–76, https://doi.org/10.1016/j.simpat.2015.03.011.
[25] Y. Wang, G. Zhao, X. Xu, X. Chen, C. Zhang, Constitutive modeling, processing map establishment and microstructure analysis of spray deposited Al-Cu-Li alloy 2195, J. Alloy. Compd. 779 (2019) 735–751, https://doi.org/10.1016/J.JALLCOM.2018.11.289.
[26] N.L. Bhirud, R.R. Gawande, F. Jafarian, Measurement and prediction of cutting temperatures during dry milling: review and discussions, J. Braz. Soc. Mech. Sci. Eng. 39 (2017) 5135–5158, https://doi.org/10.1007/s40430-017-0869-7.
[27] F. Jafarian, 3D modeling of recrystallized layer depth and residual stress in dry machining of nickel-based alloy, J. Braz. Soc. Mech. Sci. Eng. 41 (2019) 1–10, https://doi.org/10.1007/s40430-019-1707-x.
[28] N. Senthilkumar, T. Tamizharasan, Effect of tool geometry in turning AISI 1045 steel: experimental investigation and FEM analysis, Arabian J. Sci. Eng. 39 (2014) 4963–4975, https://doi.org/10.1007/s13369-014-1054-2.
[29] M.R. Stalin John, K. Shrivastava, N. Banerjee, P.D. Madhukar, B.K. Vinayagam, Finite element method-based machining simulation for analyzing surface roughness during turning operation with HSS and carbide insert tool, Arabian J. Sci. Eng. 38 (2013) 1615–1623, https://doi.org/10.1007/s13369-013-0541-1.
[30] A.K. Parida, K. Maity, Effect of nose radius on forces, and process parameters in hot machining of Inconel 718 using finite element analysis, Eng. Sci. Technol. Int. J. 20 (2017) 687–693, https://doi.org/10.1016/j.jestch.2016.10.006.
[31] M.E. Korkmaz, M. Günay, Experimental and statistical analysis on machinability of Nimonic80A superalloy with PVD coated carbide, Sigma J. Eng. Nat. Sci. 36 (2018) 1141–1152.
[32] M. Günay, M.E. Korkmaz, N. Yaşar, Finite element modeling of tool stresses on ceramic tools in hard turning, Mechanika 23 (3) (2017) 432–440, https://doi.org/10.5755/j01.mech.23.3.14363.
[33] V.D. Patel, A.H. Gandhi, Modeling of cutting forces considering progressive flank wear in finish turning of hardened AISI D2 steel with CBN tool, (2019).
[34] A. Popov, A. Dugin, Effect of uncut chip thickness on the ploughing force in orthogonal cutting, Int. J. Adv. Manuf. Technol. 76 (2015) 1937–1945, https://doi.org/10.1007/s00170-014-6423-1.
[35] J. Yang, X. Wang, M. Kang, Finite element simulation of surface roughness in diamond turning of spherical surfaces, J. Manuf. Processes 31 (2018) 768–775, https://doi.org/10.1016/J.JMAPRO.2018.01.006.
[36] K. Gok, Development of three-dimensional finite element model to calculate the turning processing parameters in turning operations, Measurement 75 (2015) 57–68, https://doi.org/10.1016/J.MEASUREMENT.2015.07.034.
[37] V. Vijayaraghavan, A. Garg, L. Gao, R. Vijayaraghavan, G. Lu, A finite element based data analytics approach for modeling turning process of Inconel 718 alloys, J. Cleaner Prod. 137 (2016) 1619–1627, https://doi.org/10.1016/j.jclepro.2016.04.010.
[38] K. Gök, A. Gök, Numeric simulation of effect on the CBN cutting tool stresses of austempering process, J. Polytechnic. 23 (2020) 37–44, https://doi.org/10.2339/politeknik.452739.
[39] T. Kıvak, Optimization of surface roughness and flank wear using the Taguchi method in milling of Hadfield steel with PVD and CVD coated inserts, Measurement 50 (2014) 19–28, https://doi.org/10.1016/J.MEASUREMENT.2013.12.017.
[40] A. Dorogoy, D. Rittel, Determination of the johnson-cook material parameters using the SCS specimen, Exp. Mech. 49 (2009) 881–885, https://doi.org/10.1007/s11340-008-9201-x.
[41] M.E. Korkmaz, Determination and verification of Johnson – Cook parameters for 430 ferritic steels via different gage lengths, Trans. Indian Inst. Met. (2019), https://doi.org/10.1007/s12666-019-01734-9.
[42] M. Akbari, S. Buhl, C. Leinenbach, K. Wegener, A new value for Johnson Cook damage limit criterion in machining with large negative rake angle as basis for understanding of grinding, J. Mater. Process. Technol. 234 (2016) 58–71, https://doi.org/10.1016/J.JMATPROTEC.2016.03.009.
[43] D.I. Lalwani, N.K. Mehta, P.K. Jain, Extension of Oxley's predictive machining theory for Johnson and Cook flow stress model, J. Mater. Process. Technol. 209 (2009) 5305–5312, https://doi.org/10.1016/J.JMATPROTEC.2009.03.020.
[44] A. Shrot, M. Bäker, Determination of Johnson – Cook parameters from machining simulations, Comput. Mater. Sci. 52 (2012) 298–304, https://doi.org/10.1016/j.commatsci.2011.07.035.
[45] A. Banerjee, S. Dhar, S. Acharyya, D. Datta, N. Nayak, Determination of Johnson cook material and failure model constants and numerical modelling of Charpy impact test of armour steel, Mater. Sci. Eng., A 640 (2015) 200–209, https://doi.org/10.1016/J.MSEA.2015.05.073.
[46] J. Che, T. Zhou, Z. Liang, J. Wu, X. Wang, An integrated Johnson-Cook and Zerilli-Armstrong model for material flow behavior of Ti–6Al–4V at high strain rate and elevated temperature, J. Braz. Soc. Mech. Sci. Eng. 40 (2018) 1–10, https://doi.org/10.1007/s40430-018-1168-7.
[47] A. Shokry, On the constitutive modeling of a powder metallurgy nanoquasicrystalline Al93Fe3Cr2Ti2 alloy at elevated temperatures, J. Braz. Soc. Mech. Sci. Eng. 41 (2019) 1–13, https://doi.org/10.1007/s40430-019-1617-y.
[48] M.E. Korkmaz, M. Günay, P. Verleysen, Investigation of tensile Johnson-Cook model parameters for Nimonic 80A superalloy, J. Alloy. Compd. 801 (2019) 542–549, https://doi.org/10.1016/J.JALLCOM.2019.06.153.
[49] Sandvik, AB Sandvik Coromant, in: SE-811 81, Sandviken, Sweden, 2012.
[50] J. Thrinadh, A. Mohapatra, S. Datta, M. Masanta, Machining behavior of Inconel 718 superalloy: effects of cutting speed and depth of cut, Mater. Today: Proc. (2019), https://doi.org/10.1016/J.MATPR.2019.10.128.
[51] M. Günay, Optimization with Taguchi method of cutting parameters and tool nose radius in machining of A 316L steel, J. Faculty Eng. Archit. Gazi Univ. 28 (2013) 437–444.
[52] E.O. Ezugwu, Z.M. Wang, A.R. Machado, The machinability of nickel-based alloys: a review, J. Mater. Process. Technol. 86 (1999) 1–16, https://doi.org/10.1016/S0924-0136(98)00314-8.
[53] S. Pervaiz, A. Rashid, I. Deiab, M. Nicolescu, Influence of tool materials on machinability of titanium- and nickel-based alloys: A review, Mater. Manuf. Processes 29 (2014) 219–252, https://doi.org/10.1080/10426914.2014.880460.
[54] C. Kalyan, G.L. Samuel, Cutting mode analysis in high speed finish turning of AlMgSi alloy using edge chamfered PCD tools, J. Mater. Process. Technol. 216 (2015) 146–159, https://doi.org/10.1016/J.JMATPROTEC.2014.09.003.
[55] A. Srivastava, R. Niranjan, Optimization of the radial cutting force in turning operation of Inconel718, Asian J. Sci. Technol. 9 (2018) 7705–7707.
[56] G. Rotella, O.W. Dillon, D. Umbrello, L. Settineri, I.S. Jawahir, Finite element modeling of microstructural changes in turning of AA7075-T651 Alloy, J. Manuf. Processes 15 (2013) 141–150, https://doi.org/10.1016/j.jmapro.2012.09.005.
[57] E.P. DeGarmo, J.T. Black, R.A. Kohser, Materials and Process in Manufacturing, Prentice-Hall Inc, New Jersey, 2013.
[58] M.E. Korkmaz, Determination of Material Constitutive Equation Parameters of Nickel Based Super Alloy (Nimonic 80A) and Investigation of Their Applicability, in: PhD Thesis, Karabük University Graduate School of Natural and Applied Sciences, 2018
[59] M.E. Korkmaz, M. Günay, Finite element modelling of cutting forces and power consumption in turning of AISI 420 martensitic stainless steel, Arabian J. Sci. Eng. 43 (2018) 4863–4870, https://doi.org/10.1007/s13369-018-3204-4.

Please cite this article as: M. E. Korkmaz, N. Yaşar and M. Günay, Numerical and experimental investigation of cutting forces in turning of Nimonic 80A superalloy, Engineering Science and Technology, an International Journal, https://doi.org/10.1016/j.jestch.2020.02.001